Article | Received 30 June 2024; Accepted 18 July 2024; Published 20 April 2025
https://doi.org/10.55092/pe20250005

Liquefaction Resistance Performance of Gravel Pile Treated Saturated Sand Site based on SPH–DEM Method

Yinqiang Liu[1,2], Zhifu Shen[1,2], Wenhao Xu[1,2], Xinlei Zhang[1,2], Zhihua Wang[1,2,*] and Hongmei Gao[1,2]

1 College of Transportation Engineering, Nanjing Tech University, Nanjing 211816, China
2 Jiangsu Province Engineering Research Center of Transportation Infrastructure Security Technology, Nanjing 211816, China

* Correspondence author; E–mail: wzhnjut@njtech.edu.cn.

Abstract: The nature of sand is fundamentally that of a discrete granular system, and its liquefaction process involves the intricate interplay of multi–scale and coupled field effects. The open–source SPH solver is employed for the development of a fluid–solid coupling calculation module, and this approach is utilized to reproduce the liquefaction responses in saturated sandy sites at macro and meso scales and to investigate the liquefaction mitigation performance of gravel piles. The study shows that under surface drainage conditions, liquefaction occurs almost simultaneously at all depths, with the excess pore pressure ratio reaching 1.0. Under dynamic loading, the normalized average coupling force of particles initially increases slowly, then quickly rises to 1.0 at the onset of liquefaction, and subsequently decreases progressively from deeper to shallower layers. Simulations of gravel piles demonstrate that under dynamic loading, the excess pore pressure ratio is only 0.6. Pore fluid in the fine sand flows towards the gravel drainage channels, reducing the accumulation of excess pore pressure and significantly enhancing soil strength, thus providing effective liquefaction resistance.

Keywords: sand liquefaction, SPH–DEM, fluid–solid coupling, local average method, liquefaction mechanism, gravel pile

1. Introduction

Liquefaction of sandy soil can lead to the loss of soil strength and stiffness, which is one reason for the damage, inclination and collapse of buildings and infrastructure during an earthquake strike. Specifically, the destruction of underground or super structures caused by sandy soil liquefaction has occurred widely worldwide, as exemplified by the 2018 Songyuan earthquake in China [1], the 2016 Kumamoto earthquake in Japan [2], the 2014 Cephalonia earthquake in Greece [3], and the 2012 Emilia–Romagna earthquake in Italy [4]. Therefore, sandy soil liquefaction has always been one of the challenging issues in geotechnical engineering. Reasonably evaluating the evolution of the properties of saturated sandy soil during the liquefaction process and its dynamic response to cyclic loading is the key to solving the problem of large deformation of liquefied sandy soil.

In recent years, the SPH–DEM coupling method has been applied to various scientific and engineering problems. The discrete average form of the Navier–Stokes equation by SPH incorporates the presence of the solid phase in the liquid phase and the momentum exchange between the two phases. Therefore, the SPH–DEM coupling method can be used as an alternative method to simulate fluids at the pore scale [5–7]. El Shamy and Sizkow [8–10] applied the local average SPH–DEM coupling model to simulate the soil liquefaction process through local averaging techniques and mature semi–empirical formulas for fluid–particle interaction. In addition, the proposed model can better predict responses under small and large strains and can be used to simulate the entire response process of saturated site soil under seismic excitation.

A numerical simulation study on the liquefaction of soil in liquefiable sites based on the SPH–DEM coupling method was carried out in this study. The macro and meso–scale mechanical characteristics during the liquefaction process were analyzed from the meso–scale of fluid–solid coupling, and the inherent mechanism of the liquefaction resistance process of gravel piles was explored.

2. SPH–DEM coupling simulation

2.1. Local averaging method for fluid description

Anderson and Jackson [11] established a two–phase model for the dynamic description of fluid–particle interaction. By introducing locally averaged variables into the control equations, the equations of motion for both the solid and liquid phases are modified to represent the momentum exchange and balance between the phases. Using the local averaging theory, the locally averaged Navier–Stokes (AVNS) equations are derived, and the continuity equation (assuming an incompressible fluid) is

$$\frac{\partial n\rho_f}{\partial t} + \nabla \cdot \left(n\rho_f \mathbf{u}_f \right) = 0 \tag{1}$$

where n represents the locally averaged porosity of the fluid, ρ_f denotes the true density of the fluid (1000 kg·m^{-3} for water), and $\mathbf{u}_f$ is the velocity vector of the fluid.

The corresponding momentum equation, taking the effect of gravity into account, is expressed as

$$\frac{\partial n\rho_f \mathbf{u}_f}{\partial t} + \nabla \cdot \left(n\rho_f \mathbf{u}_f \mathbf{u}_f \right) = -\nabla P + \nabla \cdot \boldsymbol{\tau} + \mathbf{f}_f^{\text{int}} + n\rho_f \mathbf{g} \tag{2}$$

where P represents the fluid pressure, $\boldsymbol{\tau}$ is the viscous stress tensor of the fluid, and $\mathbf{f}_f^{\text{int}}$ denotes the vector of fluid–solid interaction forces per unit volume of fluid.

2.2. Fluid–solid interaction law

In a typical water–solid particle mixture, the interaction forces primarily consist of drag force and pressure gradient force (buoyancy). Both drag and buoyancy stem from the interactions between solid particles and the surrounding fluid, facilitating momentum and energy transfer between the solid and liquid phases.

In this paper, for each solid particle, the fluid–solid interaction force $\mathbf{F}_a^{\text{int}}$ can be described as

$$\mathbf{F}_a^{\text{int}} = \mathbf{F}_a^{\text{D}} + \mathbf{F}_a^{\text{B}} \tag{3}$$

$$\mathbf{F}_a^B = V_a \rho_f \mathbf{g} \tag{4}$$

where $\mathbf{F}_a^{\mathrm{D}}$ represents the drag force on particle a, $\mathbf{F}_a^{\mathrm{B}}$ represents the buoyancy force on particle a, and V_a represents the volume of particle a.

The drag force on particles from liquid can be calculated according to the classic Ergun equation [12]:

$$\mathbf{F}_a^{\mathrm{D}} = \frac{\beta_a V_a}{1-n_a}\left(\bar{\mathbf{u}}_a^f - \mathbf{u}_a\right) \tag{5}$$

where β_a represents the interphase exchange coefficient of particle a, $\bar{\mathbf{u}}_a^f$ represents the average flow velocity of the fluid around particle a, n_a is the local average porosity of particle a, and $\mathbf{u}_a$ represents the velocity of particle a.

3. Simulation of saturated sand soil treated by gravel pile

3.1. Numerical ground model

Two saturated sand sites (with and without gravel pile, respectively) were modeled to analyze the seismic loading responses. The prototype saturated sand site had a dimension of 6 m in depth and 3.6 m × 3.6 m in the horizontal directions. According to similarity theory [13], under 600 times gravitational acceleration, the prototype site was scaled down to model dimensions of 0.01 m × 0.006 m × 0.006 m to reduce computation expense. The soil particles were modeled using the DEM, while the fluid was modeled using SPH. The particle size distribution is shown in Figure 1. A schematic of the site model is shown in Figure 2. For the model with gravel pile, a 1.8 m diameter gravel drainage channel (particle size range: 1.6 mm ~ 6mm) was placed as liquefaction resistance measure.

The model comprised two parts: the upper section of saturated sand and the lower section of bedrock for applying seismic loads. The friction coefficient is 0.5 and the rolling resistance coefficient is 0.15. The particle density is 2650 kg/m^3. The contact normal and tangential viscous damping ratios are 0.2. Contact modulus is 200 MPa and normal/tangential stiffness ratio is 0.2.

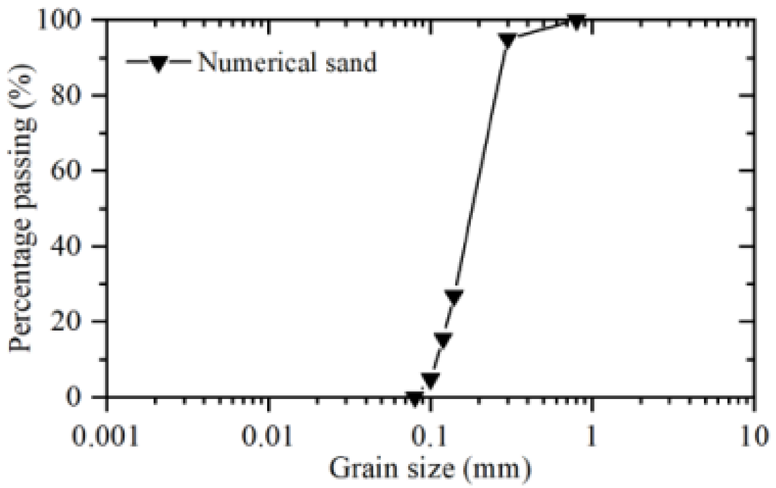

Figure 1. Particle size distribution.

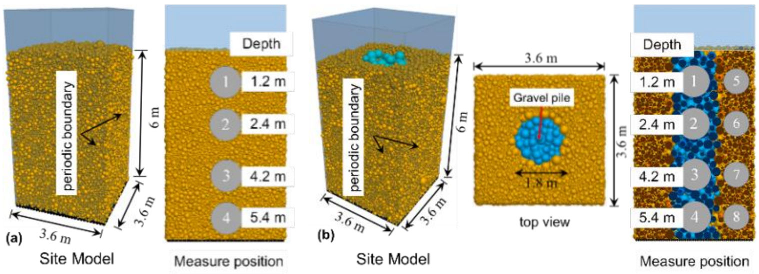

Figure 2. Saturated sand site model: **(a)** without gravel pile; **(b)** with gravel pile.

The fluid was modeled using SPH, with the initial spacing of SPH particles in the fluid domain set at 0.5 mm and a smoothing function radius of 1.5 times the particle spacing. The model was divided into boundary particles at the bottom and fluid particles at the top, with periodic boundary conditions applied on all four lateral sides. The dynamic viscosity of prototype water is 0.001 Pa s, and it is amplified to 0.60 Pa s under 600 times gravity. Xu [14] calibrated the microparameters of discrete element particles through element dynamic triaxial tests and element discrete element simulations to achieve discrete element microparameters.

The base of the saturated sand site was subjected to a sinusoidal horizontal excitation with an amplitude of 0.25 g, a frequency of 3 Hz, and a duration of 9 s. The simulation timestep is 1.0×10^{-7} s for DEM and 1.0×10^{-6} s for SPH. As shown in Figure 2, vertical monitoring points were set at various depths to measure the average acceleration of solid and fluid particles, excess pore water pressure (EPWP), average coupling force, shear stress, and shear strain during the simulation.

3.2. Seismic loading responses

Excess pore water pressure and acceleration responses. The time history curves of EPWPR (denoted by r_u hereafter) and acceleration at different depths for both model grounds are shown in Figure 3. Under excitation, r_u in the ground without gravel pile reaches 1.0 gradually and it is earlier to reach liquefaction at lower depth. The rate of excess pore pressure development in the gravel pile ground is significantly slower than that in the ground without gravel pile, and the maximum excess pore pressure achieved is also significantly lower due to the presence of gravel pile. This indicates that gravel pile can effectively inhibit the development of excess pore pressure.

As shown in Figure 3, the acceleration responses of soil layers at different depths in the ground with gravel pile are like those in the ground without gravel pile. However, the acceleration in the ground with gravel pile maintains a certain magnitude throughout the excitation process and is significantly higher than that in the ground without gravel pile at the same depths. This indicates that under the influence of gravel pile, the attenuation of shear stress and the accumulation of shear strain in the ground without gravel pile under dynamic loading are restricted.

Shear stress–strain responses of the sand. As shown in Figure 4, the cyclic shear stress–shear strain loops at various measurement points indicate that for the shallow soil layers (1.2 m and 2.4 m) in the ground without gravel pile, the shear stress initially increases and then decreases. For the deeper soil layers (4.2 m and 5.4 m), the shear stress continuously decreases before liquefaction. In contrast, at the ground with gravel pile, the shear stress in the soil at various depths does not exhibit a decreasing trend during excitation but rather continues to increase.

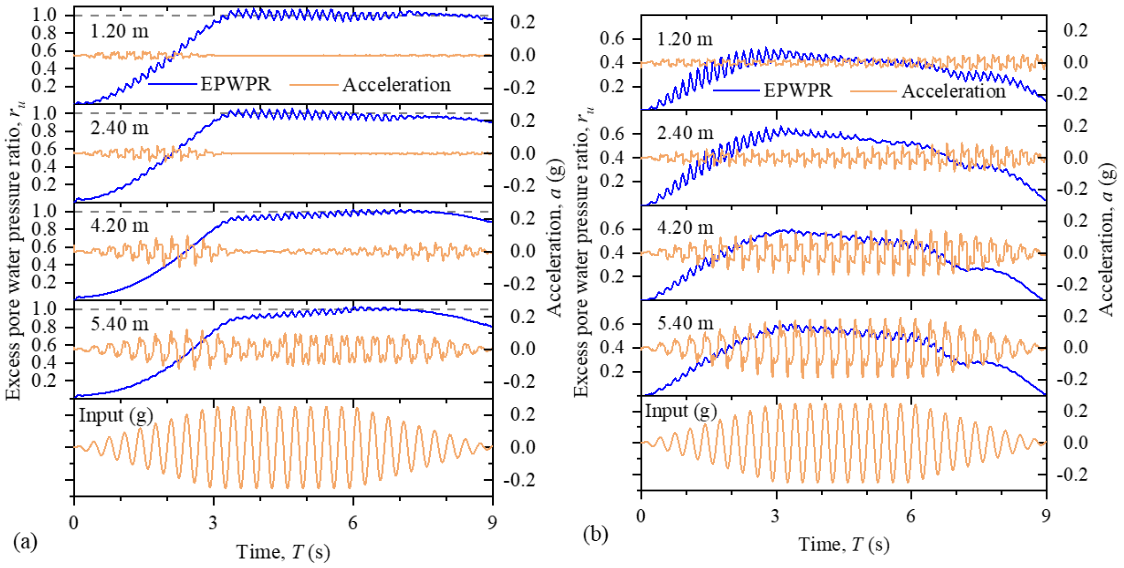

Figure 3. Time histories of excess pore water pressure ratio and acceleration at different depths: **(a)** model ground without gravel pile; **(b)** model ground with gravel pile.

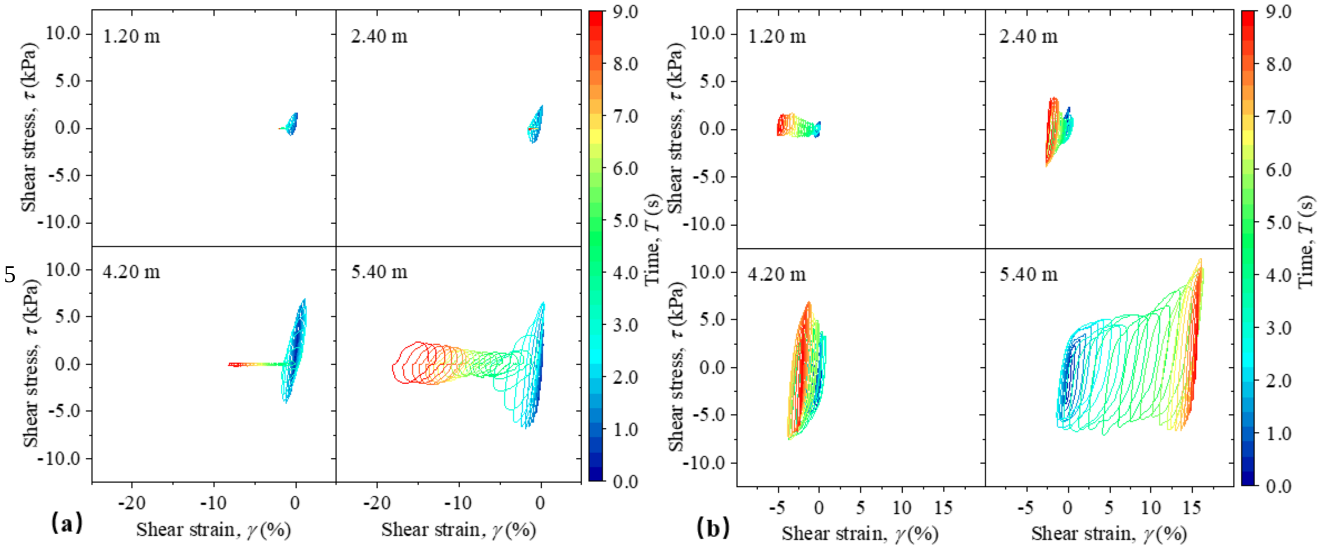

Figure 4. Shear stress–strain responses at selected depths with timescale mapped to curve color: **(a)** model ground without gravel pile; **(b)** model ground with gravel pile.

3.3. Microscopic mechanism of liquefaction resistance of gravel pile

Evolution of particle coupling force in liquefaction process. To elucidate the relationship between liquefaction phenomena and fluid–solid interactions, the normalized average coupling force of particles is defined as the ratio of the sum of coupling forces to the sum of the gravitational forces of all particles within a localized area. This normalized average coupling force characterizes the "suspension" degree of soil particles in the local area; when its value is 1, it indicates that the particles are in a "suspended" state. Figure 5 presents the time history curves of the normalized average coupling force of particles under the two conditions. In the initial stage of excitation in the saturated sand site, the normalized average coupling force develops slowly, then rises sharply, eventually reaching 1.0, indicating that the particles are suspended in the fluid, resulting in complete liquefaction. For the gravel pile–treated site, the vertical normalized average coupling force applied by the fluid to the fine sand particles at various depths is less than 1, indicating that the particles are not suspended.

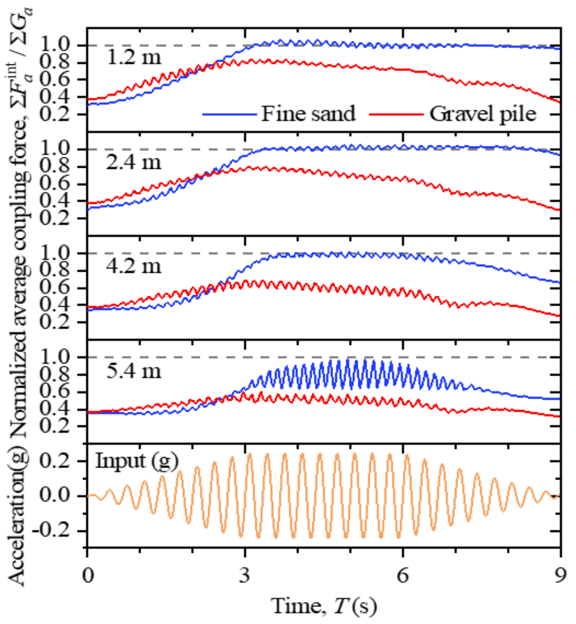

Figure 5. Time histories of normalized particle average coupling force at selected depths.

Evolutions of inter–particle contact force network. Figure 6 compares the evolution processes of the contact force chains between particles in the two ground models. As shown in Figure 6(a), the contact force chains in the ground without gravel pile are completely lost after liquefaction. Between the time of 0 s and 6 s, the contact force chains at all depths almost entirely disappear, which is the micro–mechanism behind the decay of particle acceleration after liquefaction. This is due to the reduction in dynamic load amplitude, leading to a decrease in average coupling force on particles, thus slowly increasing the contact force between particles and initiating soil skeleton re–establishment. Conversely, in the gravel pile–treated site, the contact force chains remain at a high level throughout the loading process.

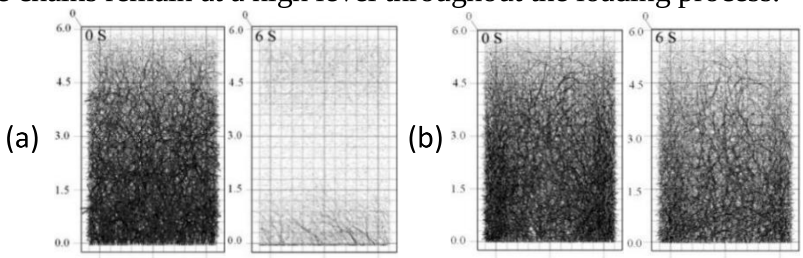

Figure 6. Evolutions of contact force chain networks: **(a)** model ground without gravel pile; **(b)** model ground with gravel pile.

Seepage behavior of pore water. Figure 7 illustrates the pore water flow velocity vectors in the central vertical cross–section at different moments during excitation for the model ground with gravel pile. Under the action of the base excitation, soil particles move horizontally with the bottom fluid, and the fluid within the sand pores flows towards the central gravel pile. As shown in the figure, the pore water within the sand almost entirely flows towards the central gravel pile, and the pore water within the gravel pile flows towards the ground top. The simulation results fully demonstrate that gravel piles have a capability by dissipate the accumulated pore pressure, thereby enhancing the ground liquefaction resistance.

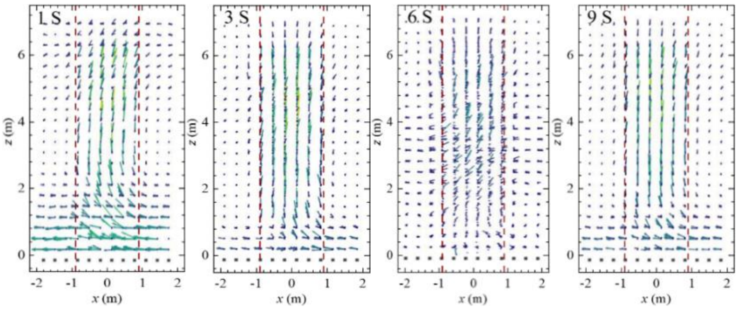

Figure 7. Pore water velocity vector at different times.

4. Conclusion

This study developed and applied SPH–DEM coupled numerical simulation technology based on a locally averaged SPH–DEM coupling calculation model. Numerical simulations of the liquefaction resistance process of gravel piles were conducted. The main conclusions are as follows.

(1) Under surface drainage conditions, the excess pore pressure ratio at various depths reaches 1.0 around 3 s, causing liquefaction almost simultaneously. During the load decaying phase, the pore pressure shows some dissipation, with deeper layers dissipating faster.

(2) The normalized average coupling force of particles characterizes the degree of "suspension" of soil particles in a local area. During dynamic loading, the normalized average coupling force initially develops slowly and then increases sharply, reaching 1.0 at the onset of initial liquefaction. With the continuation of dynamic loading, the normalized average coupling force decreases, transitioning from deeper to shallower layers with a certain time lag.

(3) The simulation results of the liquefaction resistance of gravel piles indicate that the excess pore pressure ratio in the site is only 0.6 during dynamic loading. A pressure gradient exists between the gravel channel and the fine sand, forcing pore fluid in the fine sand to flow towards the gravel drainage channel. This effectively reduces the accumulation of excess pore pressure and significantly maintains the soil strength, demonstrating that this measure effectively mitigates the liquefaction effects in liquefiable sites and has a liquefaction resistance.

Acknowledgement

This work was supported by the National Natural Science Foundation of China (51678300, 52178336, 52108324), Major Research Project in Natural Sciences for Higher Education Institutions of Jiangsu Province (18KJA560002), Young Academic Leader in the "Qinglan Project" of Universities in Jiangsu Province, Jiangsu Provincial Graduate Research and Practice Innovation Program (KYCX24_1583).

Conflicts of interests

The authors declare no conflict of interest.

Authors' contribution

Conceptualization, Yinqiang Liu and Zhifu Shen; methodology, Wenhao Xu; software, Wenhao Xu; validation, Yinqiang Liu, Zhifu Shen. and Wenhao Xu; formal analysis, Hongmei Gao; investigation, Xinlei Zhang; resources, Zhihua Wang; data curation, Wenhao Xu; writing—original draft preparation, Yinqiang Liu; writing—review and editing, Zhifu Shen; visualization, Wenhao Xu; supervision, Zhihua Wang; project administration, Zhihua Wang; funding acquisition, Hongmei Gao. All authors have read and agreed to the published version of the manuscript.

References

[1] Shao Z, Zhong J, Howell J, Hao B, Luan X, *et al*. Liquefaction structures induced by the M5.7 earth quake on May 28, 2018 in Songyuan, Jilin Province, NE China and research implication. *J. Palaeog eogr.* 2020, 9(3).
[2] Setiawan H, Serikawa Y, Nakamura M, Miyajima M, Yoshida M. Structural damage to houses and buildings induced by liquefaction in the 2016 Kumamoto Earthquake, Japan. *Geoenviron. Disasters* 2017, 4(13).
[3] Papathanassiou G, Ganas A, Valkaniotis S. Recurrent liquefaction–induced failures triggered by 2 014 Cephalonia, Greece earthquakes: Spatial distribution and quantitative analysis of liquefaction potential. *Engineering Geology* 2016, 200:18–30.
[4] Papathanassiou G, Mantovani A, Tarabusi G, Rapti D, Caputo R. Assessment of liquefaction potential for two liquefaction prone areas considering the May 20, 2012 Emilia (Italy) earthquake. *Eng. Geol.* 2015, 189:1–16.
[5] Abdelhamid Y, El S. Pore–Scale Modeling of Fine–Particle Migration in Granular Filters. *Int. J. Geomech.* 2016, 16(3):4015086.
[6] El Shamy U, Abdelhamid Y. Modeling granular soils liquefaction using coupled lattice Boltzman n method and discrete element method. *Soil Dyn. Earthquake Eng.* 2014, 67:119–132.
[7] Han Y, Cundall P. Lattice Boltzmann modeling of pore–scale fluid flow through idealized porous media. *Int. J. Numer. Methods Fluids* 2011, 67(11):1720–1734.
[8] El Shamy U, Sizkow SF. Coupled smoothed particle hydrodynamics–discrete element method simulations of soil liquefaction and its mitigation using gravel drains. *Soil Dyn. Earthquake Eng.* 2021, 140:106460.
[9] El Shamy U, Sizkow SF. Coupled SPH–DEM simulations of liquefaction–induced flow failure. *Soil Dyn. Earthquake Eng.* 2021, 144:106683.
[10] Sizkow SF, El Shamy U. SPH–DEM simulations of saturated granular soils liquefaction incorpora ting particles of irregular shape. *Comput. Geotech.* 2021, 134:104060.
[11] Anderson T, Jackson R. A Fluid Mechanical Description of Fluidized Beds. Equations of Motion. *Ind. Eng. Chem. Fundam.* 1967, 6(4):527–539.
[12] Ergun S. Fluid flow through packed columns. *Chem. Eng. Prog.* 1952, 2(48):89–93.
[13] Kutter, B. Dynamic centrifuge modeling of geotechnical structures. *Transp. Res. Rec*. 1992, 1336:24–30.
[14] Xu W, Wang Z, Shen Z, Gao H, Liu Y, *et al*. Simulation of saturated sand site liquefaction based on the CFD–DEM method (in Chinese). *Rock Soil Mech.* 2024, 08:1–11.